

Finite Beam Depth Analysis for Large Arrays

Alva Kosasih, Emil Björnson, *Fellow, IEEE*

Abstract

Most wireless communication systems operate in the far-field region of antennas and antenna arrays, where waves are planar and beams have infinite depth. When antenna arrays become electrically large, it is possible that the receiver is in the radiative near-field of the transmitter, and vice versa. Recent works have shown that near-field beamforming exhibits a finite depth, which enables a new depth-based spatial multiplexing paradigm. In this paper, we explore how the shape and size of an array determine the near-field beam behaviors. In particular, we investigate the 3 dB beam depth (BD), defined as the range of distances where the gain is greater than half of the peak gain. We derive analytical gain and BD expressions and prove how they depend on the aperture area and length. For non-broadside transmissions, we find that the BD increases as the transmitter approaches the end-fire direction of the array. Furthermore, it is sufficient to characterize the BD for a broadside transmitter, as the beam pattern with a non-broadside transmitter can be approximated by that of a smaller/projected array with a broadside transmitter. Our analysis demonstrates that the BD can be ordered from smallest to largest as ULA, circular, and square arrays.

Index Terms

Beam depth, beam width, radiative near-field, Fresnel region, finite-depth beamforming, rectangular arrays, circular arrays.

I. INTRODUCTION

Thanks to the successful implementation of massive multiple-input multiple-output (M-MIMO) in 5G systems in sub-6 GHz and mm-wave bands [2], it is likely that even larger arrays (e.g., extremely large aperture arrays [3], [4] and holographic MIMO [5]) and wider spectrum at higher frequencies [6], [7] will be employed in the next generation of wireless systems [8], [9]. A higher

Parts of this paper have been submitted for potential publication at the 2023 IEEE Global Communications Conference (Globecom) [1]. A. Kosasih and E. Björnson are with the Division of Communication Systems, KTH Royal Institute of Technology, Stockholm, Sweden. E-mail: {kosasih,emilbjo}@kth.se. This paper was supported by the Grant 2019-05068 from the Swedish Research Council.

carrier frequency implies a smaller wavelength and, therefore, a smaller antenna size. As the array's aperture grows and the wavelength shrinks, the traditional far-field distance boundary, known as the Fraunhofer distance, will be very large since it is proportional to the squared aperture length and inversely proportional to the wavelength. Hence, future wireless systems are unlikely to operate in the far field and the signal processing must be redesigned to not rely on the far-field assumption. For instance, far-field configured arrays feature significant array gain degradation when used in the near-field [10].

Three regions have been defined to classify the wavefront behavior with respect to the distance between the transmitter and receiver [11]: the reactive near-field, the radiative near-field, and the far-field [12]. The latter two are of interest for long-range communications, as in mobile networks. At the beginning of the radiative near-field, there are discernible and unavoidable amplitude variations over the wavefront, but the main property is the spherical phase variations because these can be managed through refined signal processing. In the far-field, both the amplitude and phase variations are insignificant. In line with this, [13] suggested that conventional modeling assumptions, which include the assumption of uniform plane wave impingement, are no longer applicable when considering a large array. In particular, their research focuses on the mathematical modeling and performance analysis of extra-large arrays. They have developed a closed-form expression for the resulting signal-to-noise ratio (SNR) using optimal single-user maximum-ratio combining/maximum-ratio transmission beamforming techniques. Similarly, [14] suggested that an exact near-field channel model is needed to evaluate spectral efficiency with the perspective of interference suppression capability.

A. Related Works

Previously negligible propagation phenomena become dominant in the near-field. In conventional far-field beamforming, the signal in line-of-sight scenarios is focused on a point that is infinitely far away, resulting in a directive beam with a limited angular width but continuing to infinity. In the near-field, we can aim the radiated signal at a specific point in space and achieve a radiation pattern that focused around it, both angle and depth. This is known as beamforming in the distance domain or finite-depth beamforming [8], [15]–[21]. In other words, near-field beamforming enables one to configure the beam not only in the angular domain (beam width) but also in the distance domain (beam depth). Focusing signal at a specific location can be

performed by utilizing a matched filter that takes into consideration the phase shift of each individual element present in the array.

The concept of finite-depth near-field beamforming was first introduced in [8]. The fundamental properties can be studied using continuous matched filtering, representing the case when the array consists of many small elements so that summations over the antennas can be expressed using integrals [22]–[24]. Since then, researchers have conducted numerous studies utilizing the limited-depth capability of near-field beamforming. In [15], the focusing property was utilized to derive the closed-form array response, which is then used to develop an effective method for location and channel parameters estimation. Similarly, [16] proposed the focal scanning method for sensing the location of the receiver, based on the analytic expression of the reflection coefficient of a reflective intelligent surface. [17] proposed a near-field channel estimation using a polar domain representation to accommodate both the angular and distance domains. Similarly, [18] proposed location division multiple access (LDMA) to enhance spectrum efficiency compared to classical spatial division multiple access (SDMA). The LDMA exploited extra spatial resources in the distance domain to serve different users at different locations in the near field. [19], [20] further analyzed the near-field beam for massive wideband phased arrays. The focus of their work was to develop a low-complexity technique for constructing beams, which is particularly suitable for massive wideband phased arrays.

Despite the growing interest in near-field beamforming, there have been no investigations reported on the near-field beam radiation pattern in the distance domain, referred to as the beam depth (BD), except for the recent study [21]. Understanding the near-field beam radiation pattern is crucial because it enables us to optimize beamforming system performance and accuracy. For example, the behavior of the BD can provide insights into how to spatially multiplex users in the depth domain with minimal interference, and what array geometries to use. [21] characterized the BD including the distance interval where the array gain is within 3 dB from the peak value. However, the analysis is restricted to a square array with a transmitter in the broadside direction. We note that the antenna array geometry can be optimized to make the most out of the finite BD property of near-field beamforming.

B. Contributions

In this paper, our objective is to extend the understanding of near-field beamforming by considering a rectangular array model with a tunable width-to-height proportion. In particular,

we investigate the array gain and BD. We analytically derive the array gain and BD using the Fresnel approximation, which is demonstrated to be an accurate and reliable method in our analysis. Using these derived expressions, we explore how various geometrical factors, such as the width-to-height proportion, area, and aperture length, affect the array gain and BD of rectangular arrays. We further consider rectangular arrays with a non-broadside transmitter and analyze how the array gain and BD are affected by the azimuth angle. Moreover, we extend the analysis by considering near-field beamforming with a circular array, and showcase the potential advantages and limitations compared with rectangular arrays. Finally, to better understand the beam behaviors in the distance domain, we analyze the nulls and sidelobes appearing as a function of the propagation distance.

There are four main contributions of this paper:

- We analyze the BD for broadside beamforming with respect to the rectangular array shape and size. The analysis is performed by deriving the normalized array gain, computing the BD analytically, and obtaining the upper finite BD limit. The analysis allows us to characterize the finite-depth beam behavior in the near-field and how the array geometry can be tuned to achieve preferred properties. This analysis can be used to define beam orthogonality in the spatial domain.
- We extend the analysis to consider non-broadside beamforming, in which case direct Fresnel approximations are highly inaccurate. We refine the approximation to obtain high accuracy and then derive the analytical array gain with respect to the azimuth angle. Furthermore, we analyze the BD with respect to the azimuth angle.
- We analyze the BD for a circular array. The analysis is performed by deriving the normalized array gain, computing the BD analytically, and obtaining the upper finite BD limit. Furthermore, we characterize the beam behaviors outside the mainlobe in the distance domain by analyzing the nulls and sidelobes as a function of the propagation distance. The results provide insights into how such sidelobes may interfere with the other users' signals.
- We investigate the possibility that a non-broadside transmitter array can be modeled as a smaller array with a broadside transmitter by projecting it onto a plane perpendicular to the axis of the non-broadside transmitter. Our results confirm that the approximation is sufficiently accurate, as it closely matches the exact gain obtained from the non-broadside transmitter array.

The paper is organized as follows. In Section II, we provide preliminaries and definitions for an individual antenna and antenna array. In Section III, we derive the gain and BD of rectangular arrays with a broadside transmitter and analyze its properties. In Section IV, we analyze the gain and BD of rectangular arrays with a non-broadside transmitter. In Section V, we derive the gain and BD of a circular array. This paper is concluded in Section VI.

II. PRELIMINARIES

In this section, we discuss the behavior of electromagnetic radiation from a passive antenna and an antenna array. Three regions classically define the electromagnetic radiation patterns with respect to the propagation distance: the reactive near-field, radiative near-field, and far-field.

A. Gain of a Passive Antenna

The reactive near-field of a large antenna with an aperture length of D spans from $z = 0$ to $z \approx 0.62\sqrt{D^3/\lambda}$ [21], where z is the distance from the antenna and λ is the wavelength. The radiative near-field, also known as the Fresnel region, starts roughly where the reactive near-field ends, i.e., from $z = 1.2D$ to $z = d_F$ [21], where

$$d_F = \frac{2D^2}{\lambda}, \quad (1)$$

is the Fraunhofer distance [12], obtained by using a Taylor approximation with an assumption that a phase difference of $\frac{\pi}{8}$ over the aperture is negligible when analyzing the gain.

These definitions are based on classical approximation, which might not be well-tuned for future systems. It is therefore essential to begin our new analysis from electric field expressions. We consider a free-space propagation scenario, where there exists an isotropic transmitter located at (x_t, y_t, z) and a planar receiver centered at the origin covering an area denoted as \mathcal{A} in the xy -plane. When the transmitter emits a signal with polarization in the y -dimension, the electric field at the point $(x, y, 0)$ of the receiver aperture becomes [24, App. A]

$$E(x, y) = \frac{E_0}{\sqrt{4\pi}} \frac{\sqrt{z(x-x_t)^2 + z^2}}{r^{5/4}} e^{-j\frac{2\pi}{\lambda}\sqrt{r}}, \quad (2)$$

where $r = ((x-x_t)^2 + (y-y_t)^2 + z^2)$ is the squared Euclidean distance between the transmitter and the considered point, and E_0 is the electric intensity of the transmitted signal in the unit of Volt. The electric field expression in (2) is valid in the Fresnel region since it takes into account

the reduction in effective area due to the incident angle, polarization mismatch, and free-space geometric path loss. The complex-valued channel response to the receive antenna can then be calculated as in [24, Eq. (64)]

$$h = \frac{1}{\sqrt{AE_0}} \int_{\mathcal{A}} E(x, y) dx dy. \quad (3)$$

Hence, the received power is computed as $E_0^2 |h|^2 / \eta$, where η is the impedance of free space. The receive antenna gain compared to an isotropic antenna is computed as [25, Eq. (6)]

$$G = \frac{|\int_{\mathcal{A}} E(x, y) dx dy|^2}{\frac{\lambda^2}{4\pi} \int_{\mathcal{A}} |E(x, y)|^2 dx dy}, \quad (4)$$

where $\frac{\lambda^2}{4\pi}$ is the area of the isotropic antenna. The antenna gain is normally analyzed in the far-field where the incident wave is plane so that $G_{\text{plane}} = \frac{4\pi}{\lambda^2} A$, where A is the physical area of the antenna element. A different value is obtained in the Fresnel region where there can be phase and amplitude variations over the aperture. In this paper, we consider the normalized antenna gain defined in [21] as

$$G_{\text{antenna}} = \frac{G}{G_{\text{plane}}} = \frac{|\int_{\mathcal{A}} E(x, y) dx dy|^2}{A \int_{\mathcal{A}} |E(x, y)|^2 dx dy}, \quad (5)$$

which compares the achieved antenna gain in the Fresnel region to the one obtained in the far field.

B. Gain of an Antenna Array

In this paper, we consider a uniform planar array (UPA) with N antenna elements, where N can be a large number. The antenna elements are uniformly distributed across the array and we consider the same number of antenna elements in the x and y dimensions. However, the elements can be rectangular, which will result in a rectangular aperture shape in the xy -plane. Each antenna element is indexed by $n \in \{1, \dots, \sqrt{N}\}$ and $m \in \{1, \dots, \sqrt{N}\}$ which are the location indexes on the x and y axes, respectively. The Fraunhofer array distance depends on the antenna/array sizes and becomes $d_{FA} = Nd_F$.

We consider the same isotropic transmitter as before but assume that the receiver is equipped with the UPA. The complex-valued channel response to a receive antenna element can then be written similarly to (3) as

$$h_{n,m} = \frac{1}{\sqrt{AE_0}} \int_{\mathcal{A}} E(x, y) dx dy, \quad (6)$$

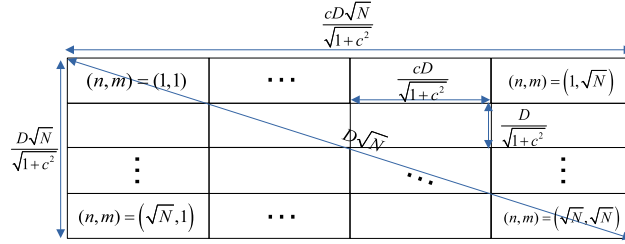


Fig. 1. We consider a generalized rectangular array design, where the width of each antenna element is c times its height. The number of elements is constant irrespective of the sizes or shapes of the elements. When changing the shape of the array, we can either fix the diagonal of the array as $D_{\text{array}} = \sqrt{N}D$ or the array's aperture area $A_{\text{array}} = NA$.

where A denotes the physical area of each antenna. If the transmitted signal has a power of E_0^2/η and matched filtering is utilized, the signal-to-noise ratio (SNR) becomes

$$\text{SNR} = \frac{E_0^2}{\eta\sigma^2} \sum_{n=1}^{\sqrt{N}} \sum_{m=1}^{\sqrt{N}} |h_{n,m}|^2, \quad (7)$$

where σ^2 denotes the receiver noise variance. Similarly to (5), we define the normalized array gain

$$G_{\text{array}} = \frac{\sum_{n=1}^{\sqrt{N}} \sum_{m=1}^{\sqrt{N}} \left| \int_{\mathcal{A}} E(x,y) dx dy \right|^2}{NA \int_{\mathcal{A}} |E(x,y)|^2 dx dy}, \quad (8)$$

which is the combined antenna and array gains achieved in the Fresnel region compared to what is achievable in the far-field.

III. GAIN AND BEAM DEPTH OF RECTANGULAR ARRAYS WITH A BROADSIDE TRANSMITTER

In this section, we consider a UPA with a rectangular shape. As illustrated in Fig. 1, the array is composed of antenna elements, each with a height of $\ell = D/\sqrt{1+c^2}$ and width of $w = c\ell$ for some $c \in \mathbb{R}_0^+$, where D denotes the diagonal. We refer to this as a *generalized rectangular array* since different shapes are obtained depending on the value of c . If we fix the array's aperture area $A_{\text{array}} = NA$, the diagonal of the array (i.e., the aperture length) becomes $\sqrt{A_{\text{array}}(1+c^2)}/c$ which varies with c . If we instead fix the array's aperture length $D_{\text{array}} = \sqrt{N}D$, the array's aperture area $c(D_{\text{array}})^2/(1+c^2)$ will depend on c . We consider both scenarios in this paper to study how the shape of the beamforming depends on the array geometry. We take the viewpoint of a receiver array with an isotropic transmitter, for ease in presentation, but the same results apply in the reciprocal setup with a transmitting array.

The antenna element with index (n, m) is located at the point $(x_n, y_m, 0)$, where

$$x_n = \left(n - \frac{\sqrt{N} + 1}{2} \right) w, \quad y_m = \left(m - \frac{\sqrt{N} + 1}{2} \right) \ell, \quad (9)$$

and covers an area of

$$\mathcal{A} = \left\{ (x, y, 0) : |x - x_n| \leq \frac{w}{2}, |y - y_m| \leq \frac{\ell}{2} \right\}. \quad (10)$$

Let us now consider the normalized array gain in (8). We can either numerically evaluate it or use a Fresnel approximation that allows us to obtain an analytical expression. In the latter case, we approximate $E(x, y)$ in (2) as

$$E(x, y) \approx \frac{E_0}{\sqrt{4\pi z}} e^{-j\frac{2\pi}{\lambda} \left(z + \frac{x^2}{2z} + \frac{y^2}{2z} \right)}. \quad (11)$$

This approximation is tight in the part of the Fresnel region where the amplitude variations are negligible over the aperture. The term $z + \frac{x^2}{2z} + \frac{y^2}{2z}$ determines the phase variations in (11) and is obtained from a first-order Taylor approximation of the Euclidean distance between transmitter and array:

$$\sqrt{x^2 + y^2 + z^2} = z \sqrt{1 + \left(\frac{x^2 + y^2}{z^2} \right)} \approx z + \frac{x^2 + y^2}{2z}. \quad (12)$$

The approximation error is small when $\frac{x^2 + y^2}{z^2} \leq 0.1745$, which results in relative errors below $3.5 \cdot 10^{-3}$ [21]. To give a concrete example, we consider a square array with $c = 1$, $N = 10^4$ antennas, and $D = 0.025$ meter. The relative error is smaller than $3.5 \cdot 10^{-3}$ if $z > 1.2D\sqrt{N}$.

Suppose the matched filtering in the array is focused on the point $(0, 0, F)$, which might be different from the location $(0, 0, z)$ of the transmitter. We will now use the Fresnel approximation in (11) to compute the normalized array gain by injecting the phase-shift $e^{+j\frac{2\pi}{\lambda} \left(\frac{x^2}{2F} + \frac{y^2}{2F} \right)}$ into the integrals in (8) to represent a continuous matched filter [22]–[24].

Theorem 1. When the transmitter is located at $(0, 0, z)$ and the matched filtering is focused on $(0, 0, F)$, the Fresnel approximation of the normalized array gain for the generalized rectangular array becomes

$$\hat{G}_{\text{rect}}(c) = \frac{(C^2(c\sqrt{a}) + S^2(c\sqrt{a}))(C^2(\sqrt{a}) + S^2(\sqrt{a}))}{(ca)^2}, \quad (13)$$

where $C(\cdot)$ and $S(\cdot)$ are the Fresnel integrals [26], $a = \frac{d_{FA}}{4z_{\text{eff}}(1+c^2)}$, and $z_{\text{eff}} = \frac{Fz}{F-z}$.

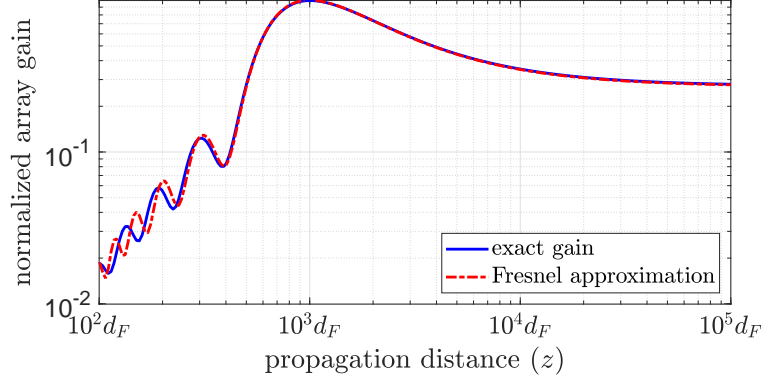


Fig. 2. The analytic approximation of the normalized array gain in Theorem 1 is compared with the exact result for a rectangular array with a broadband transmit signal and $F = 1000d_F$. We set $f_c = 3$ GHz, antenna spacing in a fraction of wavelengths $1/4$, $N = 10^4$, and $c = 4$.

Proof. The proof is provided in Appendix A and is inspired by the derivation in [26, Eq. (22)]. \square

In Fig. 2, we evaluate the tightness of the analytical expression provided in Theorem 1. We can see that the Fresnel approximation is close to the exact normalized array gain, especially when $z \geq d_B$ where $d_B = 2D\sqrt{N} = 400d_F$ denotes the Björnson distance [21] since then the amplitude variations are insignificant. Since D depends on λ , it also depends on the carrier frequency f_c . We consider $f_c = 3$ GHz in this paper. The exact normalized antenna gain is computed numerically using (8) and $E(x, y)$ as stated in (2) with the injected phase-shift $e^{+j\frac{2\pi}{\lambda}(\frac{x^2}{2F} + \frac{y^2}{2F})}$ that represents the matched filtering.

The array gain is the same irrespective of how the rectangular array is rotated in the xy -plane, which is proved as follows.

Corollary 1. The array gain expression in (13) is a symmetric function in the sense that $\hat{G}_{\text{rect}}(c) = \hat{G}_{\text{rect}}(c')$, where $c' = 1/c$.

Proof. Let us define $k \triangleq \frac{d_{\text{FA}}}{4z_{\text{eff}}}$ and $a' = \frac{d_{\text{FA}}}{4z_{\text{eff}}(1+(1/c)^2)}$. One can express $c\sqrt{a} = \sqrt{\frac{kc^2}{1+c^2}}$. If we replace c by c' , we obtain $c'\sqrt{a'} = \sqrt{\frac{k(1/c)^2}{1+(1/c)^2}} = \sqrt{\frac{k}{1+c^2}} = a$ and $\sqrt{a'} = \sqrt{\frac{k}{1+(1/c)^2}} = \sqrt{\frac{kc^2}{1+c^2}} = c\sqrt{a}$. Therefore, the numerator of (13) can also be written as $(C^2(c'\sqrt{a'}) + S^2(c'\sqrt{a'})) (C^2(\sqrt{a'}) + S^2(\sqrt{a'}))$. We notice that the denominator of (13) satisfies $(ca)^2 = (c'a')^2$. Hence, $\hat{G}_{\text{rect}}(c) = \hat{G}_{\text{rect}}(c')$. \square

Corollary 2. The array gain in (13) is an even function, i.e., $\hat{G}_{\text{rect}}(c) = \hat{G}_{\text{rect}}(-c)$.

Proof. From [26], we know that $C(c\sqrt{a})$ and $S(c\sqrt{a})$ are odd functions, that is, $C(-c\sqrt{a}) = -C(c\sqrt{a})$ and $S(-c\sqrt{a}) = -S(c\sqrt{a})$. The square of the Fresnel integrals $C^2(c\sqrt{a})$ and $S^2(c\sqrt{a})$ are both even functions since the multiplication of two odd functions gives us an even function. Therefore, $C^2(c\sqrt{a}) + S^2(c\sqrt{a}) = C^2(-c\sqrt{a}) + S^2(-c\sqrt{a})$ is an even function. The same applies to the functions $C^2(\sqrt{a}) + S^2(\sqrt{a}) = C^2(-\sqrt{a}) + S^2(-\sqrt{a})$ and $(cx)^2 = (-cx)^2$. Putting them together, we obtain $\frac{(C^2(c\sqrt{a})+S^2(c\sqrt{a}))(C^2(\sqrt{a})+S^2(\sqrt{a}))}{(cx)^2} = \frac{(C^2(-c\sqrt{a})+S^2(-c\sqrt{a}))(C^2(-\sqrt{a})+S^2(-\sqrt{a}))}{(-cx)^2}$, which proves that $\hat{G}_{\text{rect}}(c)$ is an even function. \square

The even function property of $\hat{G}_{\text{rect}}(c)$ implies that the array gain is symmetric with respect to the y -axis. We will use this property to derive an analytical expression of the BD of a rectangular array.

When applying matched filtering in the radiative near-field, the beamforming might have a limited BD; in fact, [21] advocates that the near-field ends at the point where the BD becomes infinite and not at the Fraunhofer distance. For a given focus point F , this implies that the array gain is only large for a limited range of transmitter distances z . This stands in contrast to far-field focusing where the array gain remains large in the range $z \in [F, \infty)$. We consider the 3 dB BD, $\text{BD}_{3\text{dB}}$, where the normalized array gain is higher than half of its peak gain. We will compute an analytical approximation of the BD using Theorem 1. As the peak value of $\hat{G}_{\text{rect}}(c)$ is 1, we are interested in the value of a for which $\hat{G}_{\text{rect}}(c) = 0.5$, indicating the 3 dB loss. We further denote this value of a as $a_{3\text{dB}}$, for which $\hat{G}_{\text{rect}}(c) = \hat{G}_{\text{rect}}(-c) = 0.5$ since the function is even according to Corollary 2. The precise value depends on c but can be easily computed numerically. The 3 dB BD is computed as follows by using the Fresnel approximation.

Theorem 2. The 3 dB BD of a rectangular array that is focused on $F \geq d_B$ is approximately computed as

$$\text{BD}_{3\text{dB}}^{\text{rect}} = \begin{cases} \frac{8d_{FA}F^2a_{3\text{dB}}(1+c^2)}{d_{FA}^2 - (4Fa_{3\text{dB}}(1+c^2))^2}, & F < \frac{d_{FA}}{4a_{3\text{dB}}(1+c^2)}, \\ \infty, & F \geq \frac{d_{FA}}{4a_{3\text{dB}}(1+c^2)}. \end{cases} \quad (14)$$

Proof. We can obtain a value of a from (13), for which $\hat{G}_{\text{rect}}(c)$ is approximately 0.5. The value of a is denoted as $a_{3\text{dB}}$. From Theorem 1, we know that $a_{3\text{dB}} = \frac{d_{FA}}{4z_{\text{eff}}(1+c^2)} = \frac{d_{FA}(F-z)}{4Fz(1+c^2)}$, where the value of z indicates the 3 dB gain in the propagation distance. We can then write $z = \frac{d_{FA}F}{d_{FA} + 4Fa_{3\text{dB}}(1+c^2)}$. Since $\hat{G}_{\text{rect}}(c)$ is an even function, there are two z -values resulting in the 3 dB gain. The difference between those two is the range of distances where the gain is greater

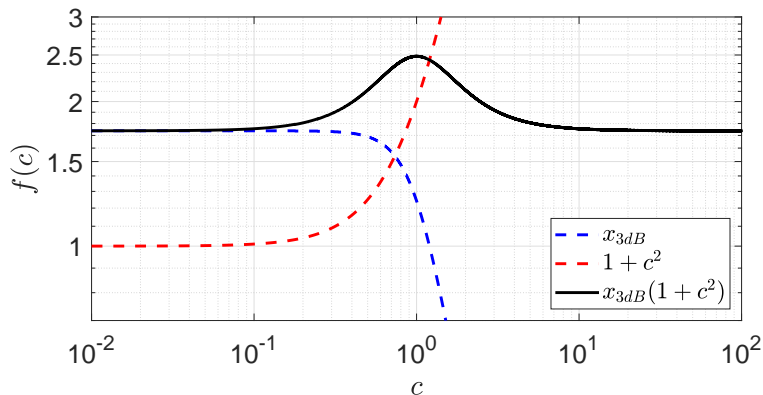


Fig. 3. The multiplication of $a_{3\text{dB}}$ and $(1 + c^2)$ with respect to c . We set $f_c = 3$ GHz, $N = 10^4$, and fixed the aperture area $A = \lambda^2/32$. The multiplication is maximized when $c = 1$.

than half of its peak gain, referred to as the 3 dB BD. Therefore, the 3 dB BD is computed as $\frac{d_{FA}F}{d_{FA}-4Fa_{3\text{dB}}(1+c^2)} - \frac{d_{FA}F}{d_{FA}+4Fa_{3\text{dB}}(1+c^2)}$ which results in (14). When $F \geq \frac{d_{FA}}{4a_{3\text{dB}}(1+c^2)}$, one of the z -values is negative which implies there is no upper limit on the beamwidth. \square

The fact that the BD is finite in the radiative near-field enables spatial multiplexing of closely spaced users, even in the same angular direction. It is essential to understand which array geometry makes this feature most prevalent.

$\text{BD}_{3\text{dB}}^{\text{rect}}$ in Theorem 2 is maximized when $c = 1$. The 3 dB BD depends on the value of $a_{3\text{dB}}$ for which $\hat{G}_{\text{rect}}(c) = 0.5$. Since it is difficult to get a closed-form solution of $a_{3\text{dB}}$ with respect to c , we simulate it as given in Fig. 3. $a_{3\text{dB}}$ is a decreasing function while $(1 + c^2)$ is an increasing function. Multiplying them together results in a function maximized when $c = 1$. Since the numerator and denominator in $\text{BD}_{3\text{dB}}^{\text{rect}}$ are maximized when the multiplication result of $a_{3\text{dB}}$ and $1 + c^2$ is maximum, the largest value of $\text{BD}_{3\text{dB}}^{\text{rect}}$ is obtained when $c = 1$.

We obtain a square array when $c = 1$ and then $\text{BD}_{3\text{dB}}^{\text{rect}} = \frac{20d_{FA}F^2}{d_{FA}^2 - 100F^2}$, which is exactly the expression of the BD in [21, Eq. (23)]. Another property from the analytical 3dB BD in (14) is that it goes to infinity when the focus distance F is greater than $\frac{d_{FA}}{4a_{3\text{dB}}(1+c^2)}$. We refer to this focus boundary as the *finite BD limit* and stress that it separates the near-field and far-field propagation characteristics. To study this limit, we plot its value in Fig. 4 as a function of c . When doing so, there are two options. We can either fix the aperture length or the total aperture area to observe how the finite BD limit depends on c . If we fix the aperture area as $A_{\text{array}} = N\lambda^2/32$, the aperture length varies with respect to c such that $\sqrt{A_{\text{array}}(1+c^2)}/c$. Since $d_{FA} = Nd_F$, where $d_F = \frac{2D^2}{\lambda}$, the finite BD limit $\frac{d_{FA}}{4a_{3\text{dB}}(1+c^2)}$ highly depends on the changes of the aperture length

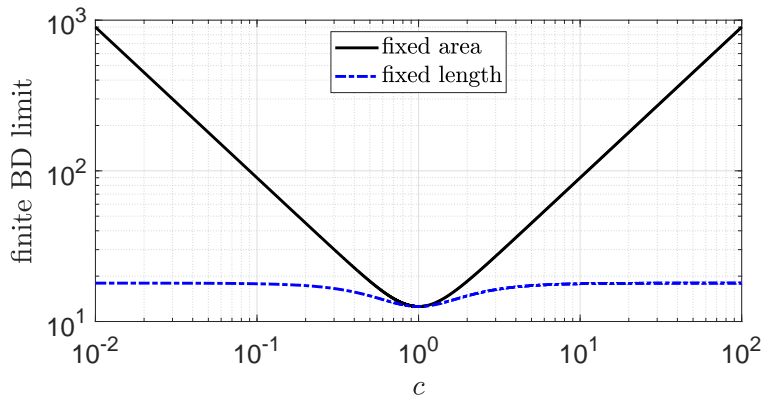


Fig. 4. The finite BD limit with respect to c . The limit indicates the boundary for the distance to the focus point F where the BD becomes infinity. We set $f_c = 3$ GHz, $N = 10^4$. The finite BD limit is minimized when $c = 1$.

D_{array} , as demonstrated in Fig. 4. The finite BD limit is minimized when $c = 1$. If we fix the aperture length $D_{\text{array}} = \sqrt{N}\lambda/4$, the limit now depends on $a_{3\text{dB}}(1 + c^2)$. More specifically, they are inversely proportional. The finite BD limit is still minimized when $c = 1$. We summarize these important results as follows.

Observation 1. The finite BD limit mostly depends on the aperture length D_{array} . Finite-depth beamforming is achievable at further distances the greater the value of D_{array} is. The finite BD regime is largest for a uniform linear array (ULA).

In the following, we numerically compute the 3 dB BD of the rectangular array with respect to c . We consider both fixed area and length scenarios.

A. Fixed Array Aperture Area vs. Fixed Array Aperture Length

When varying the shape of the antenna elements through c , we can fix the array's aperture area $A_{\text{array}} = N\lambda^2/32$, while letting the array's aperture length $D_{\text{array}} = A_{\text{array}}(1 + c^2)/c$ vary. Alternatively, we can fix the aperture length $D_{\text{array}} = \sqrt{N}\lambda/4$ so that the aperture area depends on c as $c(D_{\text{array}})^2/(1 + c^2)$. We will analyze both cases below.

Fig. 5 depicts the 3 dB BD with respect to c for a fixed area. The normalized array gain is computed numerically using (8). The 3 dB BD is maximum when the array is square-shaped ($c = 1$), i.e., around $400d_F$. The BD pattern is symmetric for tall ($c < 1$) and wide ($c > 1$) arrays, which is aligned with Corollary 1. Note that as c attains a smaller/bigger value, the two-dimensional UPA gradually approaches the shape of a one-dimensional ULA. In fact, the ULA can be regarded as a special case of our generalized rectangular array model that is achieved

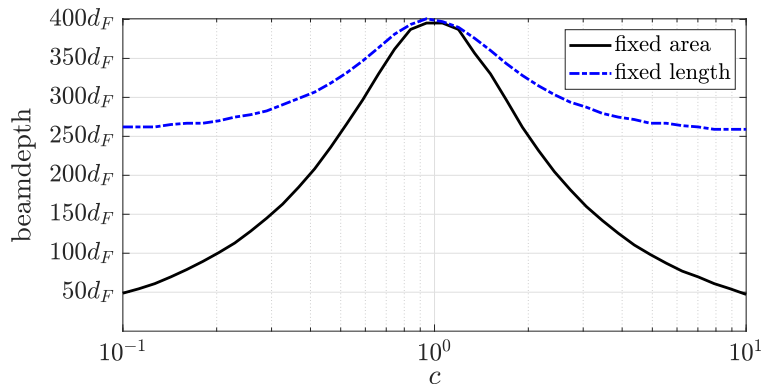


Fig. 5. The BD with respect to rectangular array shapes. We set $f_c = 3$ GHz, $N = 10^4$. The BD pattern is symmetric for tall ($c < 1$) and wide ($c > 1$) arrays, and its largest point is when $c = 1$.

when the height approaches the aperture length: $\lim_{c \rightarrow 0} \frac{D_{\text{array}}}{\sqrt{1+c^2}} = D_{\text{array}}$. The smallest BD is obtained in Fig. 5 when the array approaches a ULA with around $50d_F$ when $c = 0.1$ and $c = 10$.

Suppose we instead fix the array's aperture length so that the aperture area depends on c . The 3 dB BD for this case is also plotted in Fig. 5 with respect to c . Similarly to the results when we fix the aperture area, the 3 dB BD is maximum when the array is square-shaped ($c = 1$), i.e., around $400d_F$; The BD pattern is symmetric for tall and wide arrays, and the smallest BD is obtained when the array approaches a ULA with around $250d_F$, when $c = 0.1$ and $c = 10$. It is worth noting that the gap between the highest and smallest 3 dB BD over c for a fixed aperture length is much lower than the one in the fixed area scenario. This implies that the array's aperture length has a more significant impact on the 3 dB BD than the array area.

Observation 2. The largest 3 dB BD is obtained with a square array ($c = 1$). For tall ($c < 1$) and wide ($c > 1$) arrays, the BD patterns are symmetric. The smallest BD is obtained when the array approaches a ULA. The array's aperture length has a more significant impact on the 3 dB BD variation than the array's aperture area.

IV. GAIN AND BEAM DEPTH OF RECTANGULAR ARRAYS WITH A NON-BROADSIDE TRANSMITTER

In this section, we consider rectangular UPAs with a transmitter located in a non-broadside direction. Consequently, there will be reductions in the effective area due to directivity, as well as polarization losses. The analysis is carried out by considering a non-zero azimuth angle, but the same methodology can also be applied to consider a non-zero elevation angle. When denoting

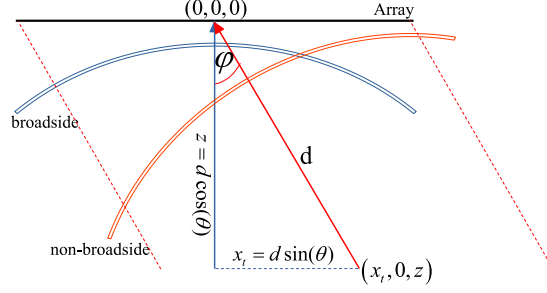


Fig. 6. The non-broadside transmitter with a rectangular array at the receiver. The transmitter is located at the distance d with an azimuth angle of φ from the center of the receiver array.

the non-zero azimuth angle as φ , the location coordinate of the transmitter is $(x_t, 0, z)$, where $x_t = d\sin(\varphi)$, $z = d\cos(\varphi)$, and d represents the distance of the transmitter to the array's center, as shown in Fig. 6. We utilized the rectangular array design discussed in the preceding section.

We first evaluate the first-order Taylor approximation of the Euclidean distance between the transmitter and receiver when the transmitter is off the center of the array's broadside direction. The Euclidean distance determines the phase variations in each antenna element of the array. Therefore, an accurate approximation of the Euclidean distance results in an accurate approximation of the array gain. The Euclidean distance between the transmitter and an antenna element located at $(x_n, y_m, 0)$ is calculated as $f_{n,m}(z) = \sqrt{(x_n - x_t)^2 + y_m^2 + z^2} = z\sqrt{1 + \frac{(x_n - x_t)^2 + y_m^2}{z^2}}$. The first-order Taylor approximation of the Euclidean distance is $\tilde{f}_{n,m}(z) = z\left(1 + \frac{(x_n - x_t)^2 + y_m^2}{2z^2}\right)$. This approximation is tight when $\frac{(x_n - x_t)^2 + y_m^2}{z^2}$ is small (e.g., ≤ 0.1745) as mentioned in Section III. However, since $z = d\cos(\varphi)$, the approximation will be significantly imprecise when φ approaches $\pm\pi/2$. We can mathematically express the above case as $\lim_{\varphi \rightarrow \pm\pi/2} \frac{(x_n - x_t)^2 + y_m^2}{(d\cos(\varphi))^2} = \infty$. To evaluate this, we first calculate the mean absolute error of the antenna elements in the array as $\epsilon = \frac{1}{N} \cdot \sum_{n=1}^{\sqrt{N}} \sum_{m=1}^{\sqrt{N}} \left| f_{n,m}(z) - \tilde{f}_{n,m}(z) \right|$, where the subscripts $n, m \in \{1, \dots, \sqrt{N}\}$ are the location indices of the antennas and $z = d_B$. Then, we plot ϵ with respect to φ demonstrated by the blue curve in Fig. 7, which we refer to as the *direct approximation*. The curve implies that the approximation is below the threshold $3.5 \cdot 10^{-3}$ for $-\pi/16 \leq \varphi \leq \pi/16$. As φ approaches $\pm\pi/8$, the approximation error exhibits a steep incline. We obtain a better approximation by first

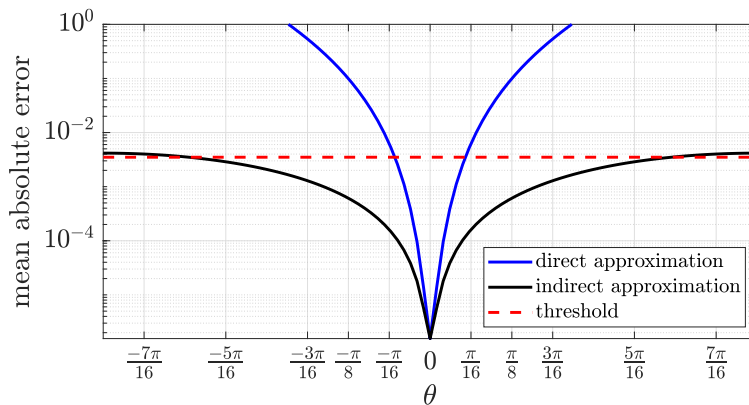


Fig. 7. The evaluation of the Euclidean distance approximations for various azimuth angles φ . The mean absolute error is obtained by computing the average absolute difference between the exact Euclidean distance and its approximation. We set $f_c = 3$ GHz, $N = 10^4$, $c = 1$, $D = \lambda/4$, and $d = 2500d_F$. The threshold is set to be $3.5 \cdot 10^{-3}$.

manipulating the expression of the Euclidean distance between the transmitter and receiver as

$$\begin{aligned}
 z \sqrt{1 + \frac{(x - x_t)^2 + y^2}{z^2}} &= z \sqrt{\underbrace{1 + \tan^2(\varphi)}_{1/\cos^2(\varphi)} + \frac{x^2 + y^2}{(d \cos(\varphi))^2} - \frac{2x \tan(\varphi)}{d \cos(\varphi)}} \\
 &= d \underbrace{\sqrt{1 + \left(\frac{x^2 + y^2 - 2xd \sin(\varphi)}{d^2} \right)}}_{f_{n,m}(d)}. \tag{15}
 \end{aligned}$$

Then, we approximate it using the first-order Taylor approximation as

$$\tilde{f}_{n,m}(d) = d + \frac{x^2 + y^2 - 2xd \sin(\varphi)}{2d}. \tag{16}$$

Now, the approximation is tight when $\frac{x^2 + y^2 - 2xd \sin(\varphi)}{d^2}$ is small and there is no $\cos(\varphi)$ -term in the denominator in contrast to $\tilde{f}_{n,m}(z)$. We refer to this approximation as the *indirect approximation*, since we manipulate the Euclidean distance expression before then applying the Taylor approximation. The corresponding mean absolute error is $\epsilon = \frac{1}{N} \cdot \sum_{n=1}^{\sqrt{N}} \sum_{m=1}^{\sqrt{N}} |f_{n,m}(d) - \tilde{f}_{n,m}(d)|$. The new approximation is evaluated in Fig. 7, where it shows that $\tilde{f}_{n,m}(d)$ (indirect approximation) is much more precise than $\tilde{f}_{n,m}(z)$ (direct approximation). For the remainder of this section, we will use the indirect approximation to approximate the Euclidean distance between the transmitter and receiver.

We further evaluate the Euclidean distance approximation with respect to the distance d and width-to-height proportion c . Fig. 8 shows that for a tall array (e.g., $c = 0.1$), the mean absolute error ϵ is below $3.5 \cdot 10^{-3}$ even for a relatively large values of φ such as $\pi/3$, with distance

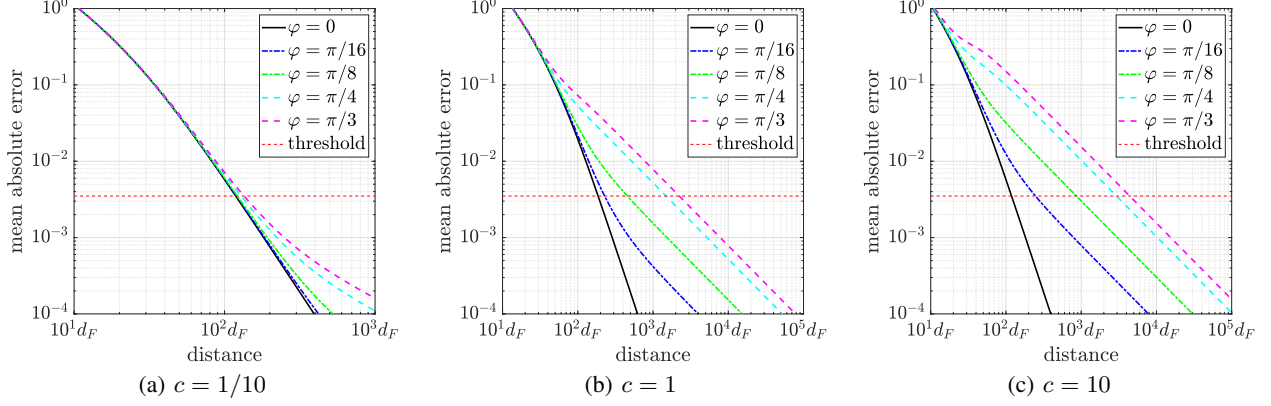


Fig. 8. Evaluation of the Euclidean distance approximations for different azimuth angles $\varphi \in \{0, \frac{\pi}{16}, \frac{\pi}{8}, \frac{\pi}{4}, \frac{\pi}{3}\}$ and rectangular array shapes, such as tall ($c < 1$), square ($c = 1$), and wide ($c > 1$). The threshold of error is $3.5 \cdot 10^{-3}$.

smaller than $1000d_F$. As c increases, the approximation error also increases. On the other hand, as the propagation distance increases, the approximation error decreases.

In the following, we will use the approximation $\tilde{f}_{n,m}(d)$ to derive an analytical normalized array gain approximation. The Fresnel approximation for the rectangular array with a non-broadside transmitter is written as

$$E(x, y) \approx \frac{E_0}{\sqrt{4\pi z}} e^{-j\frac{2\pi}{\lambda} \left(d + \frac{x^2 + y^2 - 2xd \sin(\varphi)}{2d} \right)}. \quad (17)$$

We assume that the matched filtering of the array is directed towards the point $(0, 0, F)$, which could potentially differ from the actual transmitter location $(x_t, 0, z)$. We utilize the Fresnel approximation in (17) to calculate the normalized array gain by injecting the phase-shift $e^{+j\frac{2\pi}{\lambda} \left(\frac{x^2}{2F} + \frac{y^2}{2F} \right)}$ into the integrals in (8).

Theorem 3. When the transmitter is located at $(x_t, 0, z)$ and the matched filtering is focused on $(0, 0, F)$, the Fresnel approximation of the normalized array gain for the generalized rectangular array becomes

$$\tilde{G}_{\text{rect}}(c, \varphi) = \frac{((C^2(p) + S^2(p)))}{(2cp^2)^2} ((C(cp + q) + C(cp - q))^2 + (S(cp + q) + S(cp - q))^2), \quad (18)$$

where $p = \frac{1}{2} \sqrt{\frac{d_{FA}}{d_{\text{eff}}(1+c^2)}}$, $q = \frac{x_t}{d\pi} \sqrt{2\lambda d_{\text{eff}}} = \frac{\sin(\varphi)}{\pi} \sqrt{2\lambda d_{\text{eff}}}$, and $d_{\text{eff}} = \frac{Fd}{|F-d|}$.

Proof. The proof is provided in Appendix B. \square

Fig. 9 presents an evaluation of the accuracy of the analytical expression stated in Theorem 3.

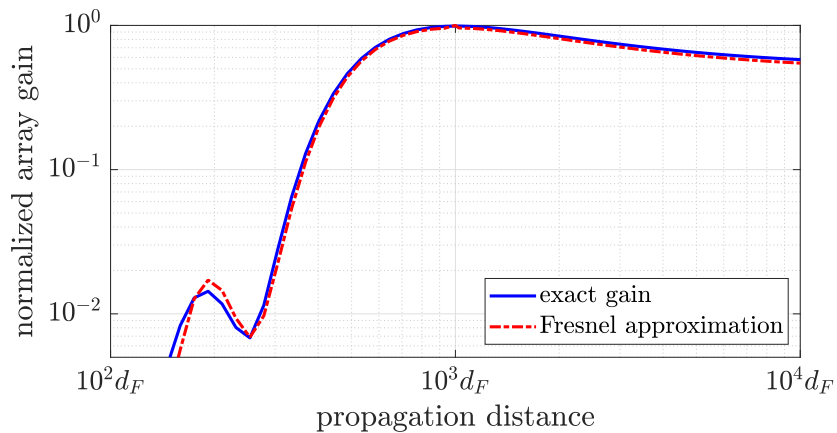


Fig. 9. The Fresnel approximation of the normalized array gain for a non-broadside transmitter with $\varphi = \pi/16$ and focus on $(0, 0, 1000d_F)$. We set $c = 1$, $N = 10^4$, and $D = \lambda/4$.

It is observed that the Fresnel approximation in Theorem 3 closely approximates the normalized array gain. The normalized antenna gain is computed numerically using (8), $E(x, y)$ as in (2), and an injected phase-shift.

Theorem 3 provides a general statement about arrays with arbitrary transmitter orientations. This is in contrast to Theorem 1, in which the transmitter orientation is restricted to the broadside direction. Theorem 1 can be derived as a special case of Theorem 3, proved as follows.

Corollary 3. The normalized array gain approximation in (18) reduces to the one in (13) when $\varphi = 0$, indicating a transmitter with a broadside direction to the receiver.

Proof. When $\varphi = 0$, it follows that $\sin(\varphi) = 0$ and $\cos(\varphi) = 1$. Thus, $x_t = 0$ while $z = d$. Then, $p = \sqrt{\frac{d_{FA}}{4d_{\text{eff}}(1+c^2)}}$ is exactly the same expression as a . Moreover, since $x_t = 0$, $q = 0$. Substituting $p = a$ and $q = 0$ into (18) yields (13) which completes the proof. \square

The array gain is irrespective of the azimuth angle φ when $c \rightarrow 0$ (a vertical ULA). Therefore, the BD is independent of φ . We prove this statement as follows.

Corollary 4. For $c \rightarrow 0$, the normalized array gain approximation is independent of the azimuth angle φ . Thus, the BD is also independent of φ .

Proof. For $c \rightarrow 0$, we can mathematically express $\tilde{G}_{\text{rect}}(c, \varphi)$ in (18) as

$$\begin{aligned} & \lim_{c \rightarrow 0} \frac{(C^2(p) + S^2(p))}{(2cp^2)^2} ((C(cp + q) + C(cp - q))^2 + (S(cp + q) + S(cp - q))^2). \\ & = \lim_{c \rightarrow 0} (C^2(p) + S^2(p)) \times \lim_{c \rightarrow 0} \frac{((C(cp + q) + C(cp - q))^2 + (S(cp + q) + S(cp - q))^2)}{(2cp^2)^2}. \end{aligned} \quad (19)$$

We obtain the result of the first limit as $C^2\left(\sqrt{\frac{d_{FA}}{4d_{\text{eff}}}}\right) + S^2\left(\sqrt{\frac{d_{FA}}{4d_{\text{eff}}}}\right)$, which is independent of φ . To compute the second limit, we first consider $\lim_{c \rightarrow 0} C(cp + q) - \lim_{c \rightarrow 0} C(-cp + q) = \Delta$, where Δ is a very small value approaching zero. The same idea applies to $\lim_{c \rightarrow 0} S(cp + q) - \lim_{c \rightarrow 0} S(-cp + q) = \Delta$. Due to the odd function property of the Fresnel integrals, we can rewrite the second limit in (19) as

$$\begin{aligned} & \lim_{c \rightarrow 0} \frac{(C(cp + q) - C(-cp + q))^2 + (S(cp + q) - S(-cp + q))^2}{(2cp^2)^2} \\ & = \frac{(\lim_{c \rightarrow 0} C(cp + q) - \lim_{c \rightarrow 0} C(-cp + q))^2 + (\lim_{c \rightarrow 0} S(cp + q) - \lim_{c \rightarrow 0} S(-cp + q))^2}{\left(\frac{d_{FA}}{2d_{\text{eff}}} \lim_{c \rightarrow 0} \frac{c}{(1+c^2)}\right)^2} \\ & \approx \frac{\Delta^2 + \Delta^2}{\Delta^2} \left(\frac{2d_{\text{eff}}}{d_{FA}}\right)^2 = 8 \left(\frac{d_{\text{eff}}}{d_{FA}}\right)^2. \end{aligned} \quad (20)$$

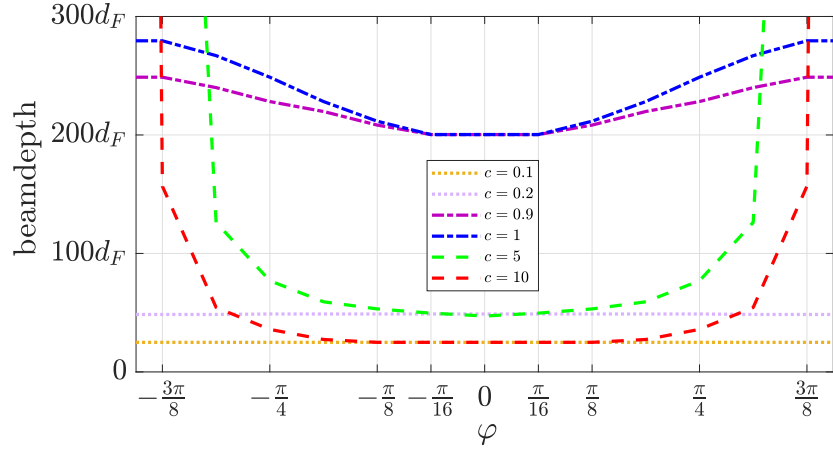
Note that (20) is also independent of φ . Therefore, (19) is independent of φ which completes the proof. \square

The reason for this result is that a vertical ULA with isotropic antennas has the same spatial resolution in all directions, as can also be observed from rotational invariance. A similar result can be proved for a horizontal ULA, which provides the same BD for any elevation angle if the azimuth angle is $\varphi = 0$.

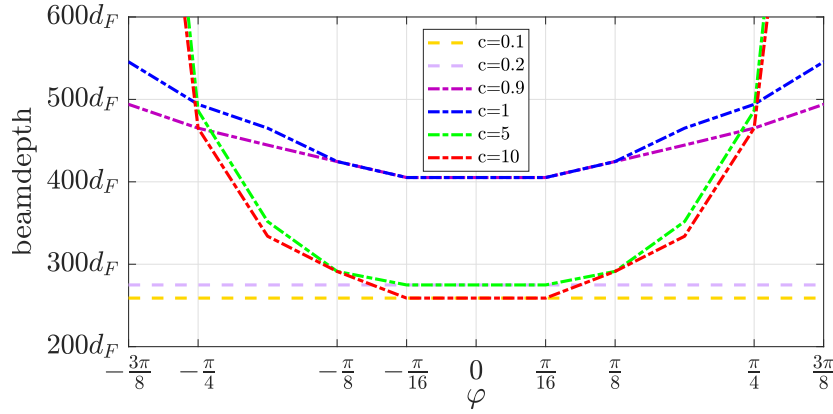
In what follows, we conduct a numerical analysis to compute the 3 dB BD of the rectangular array in the presence of a non-broadside transmitter with respect to its width/length proportion c . We consider both fixed area and length scenarios.

A. Fixed Array Aperture Area vs. Fixed Array Aperture Length

As mentioned in Section III-A, the array's aperture area can be kept constant at $A_{\text{array}} = N\lambda^2/32$ while adjusting the shape of antenna elements through c . The aperture length then



(a) The BD of rectangular arrays with a fixed area versus the azimuth angle.



(b) The BD of rectangular arrays with a fixed length versus the azimuth angle.

Fig. 10. The BD for rectangular array shapes that are either tall ($c < 1$), square ($c = 1$), or wide ($c > 1$) arrays. The BD is shown with respect to the azimuth angle for $f_c = 3$ GHz and $N = 10^4$.

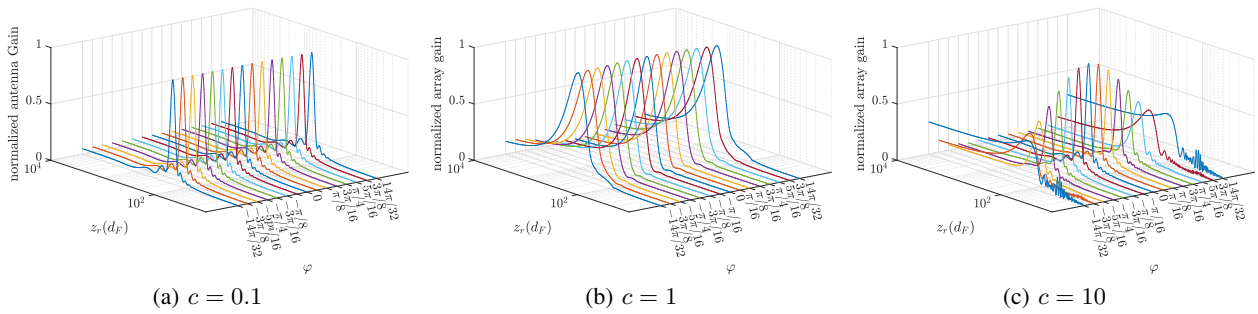
(a) $c = 0.1$ (b) $c = 1$ (c) $c = 10$

Fig. 11. The normalized array gain for different azimuth angles φ and propagation distance d . We set $f_c = 3$ GHz, $N = 10^4$, and a fixed area of $N\lambda^2/32$.

varies with c as $D_{\text{array}} = A_{\text{array}}(1 + c^2)/c$. Alternatively, fixing $D_{\text{array}} = \sqrt{N}\lambda/4$ makes the aperture area $A_{\text{array}} = c(D_{\text{array}})^2/(1 + c^2)$ dependent on c . Both cases are analyzed below.

In Fig. 10a, we plot the 3 dB BD for various rectangular array shapes with a fixed area and a transmitter located in some angular direction in the range $-3\pi/8 \leq \varphi \leq 3\pi/8$. Let us consider a BD variation, defined as the difference between the largest and smallest BD values with respect to φ , for a particular value of c . The BD variation becomes greater as c increases. When $c \rightarrow 0$, the BD variation approaches zero, implying that the BD is unaffected by the azimuth angle φ . This finding agrees with Corollary 4. For a square array ($c = 1$), the BD is around $550d_F$ for $\varphi = \pm 3\pi/8$. In the case of higher c (e.g., $c = 10$), the BD becomes much larger than $600d_F$. The latter indicates that the BD approaches infinity when $\varphi \rightarrow \pm\pi/2$. To illustrate this better, we plot Fig. 11, which shows the normalized antenna gains for a particular value of c with respect to propagation distances and azimuth angles. Fig. 11c shows a larger variation in normalized array gain compared to Figs. 11a and b. Furthermore, the BD for $\varphi = \pm 14\pi/32$ in Fig. 11c is infinite when $d \geq dB$, where the normalized array gain is around 0.3, similar to its peak.

Let us now consider the scenario where the array's aperture length is fixed, but it depends on the value of c . The 3 dB BD for various rectangular array shapes is shown in Fig. 10b. Similar to the previous scenario with a fixed aperture area, we observe that the variation in BD increases as c increases, and the BD becomes independent of the azimuth angle φ as c approaches zero. Furthermore, we observe that the highest BD values for arrays with $c = 0.1$ and $c = 1$ differ by approximately a factor of two, as the former has a value of around $550d_F$ while the latter has a value of around $260d_F$. This is in contrast to the scenario with a fixed array area, where the highest BD values for arrays with $c = 0.1$ and $c = 1$ differ by approximately a factor of eleven as the BD value of an array with $c = 0.1$ is around $560d_F$ while the one with $c = 1$ is around $50d_F$. This indicates that the aperture length is a dominant factor determining the BD.

Observation 3. As c approaches zero, so that the array approaches a vertical ULA, the BD becomes independent of the azimuth angles. For larger values of c , the BD increases with increasing azimuth angle φ , and approaches infinity as φ approaches $\pm\frac{\pi}{2}$. Finally, as the value of c increases, the BD variation also increases.

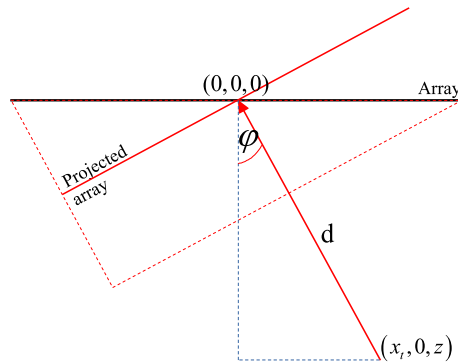


Fig. 12. The broadside transmission to a projected array. The transmitter is located at the distance d with an azimuth angle of φ from the center of the receiver array.

B. Projected Rectangular Array

In this section, we investigate the feasibility of approximating the gain that a rectangular array achieves with a non-broadside transmitter using a smaller array with a broadside transmitter. The smaller array is obtained by projecting the original array at an angle of φ . The projected array is perpendicular to the transmitter's axis, as shown in Fig. 12. Notably, the width of the projected array appears shorter by a factor of $\cos(\varphi)$, while the array's height remains unchanged. To evaluate the tightness of the approximation, we plot the normalized array gain versus the propagation distance in Fig. 13a. We can see that the approximation matches the exact gain of an array with a non-broadside transmitter when the propagation distance $d > 200d_F$, while they are slightly different for $100d_F \leq d < 200d_F$. As shown in Fig. 13b, when evaluating the tightness of the approximation at $\varphi = \pi/4$, a similar pattern is observed as in the evaluation at $\varphi = \pi/8$. Although there exists a minor discrepancy between the exact gain and the approximation, the two values are still closely matched. We further evaluate the approximation with respect to the azimuth angle φ by plotting the absolute difference of the exact and approximation gain in Fig. 13c. The approximation increases with φ . Nevertheless, the error is below 0.1, which is relatively small. This indicates that the approximation is accurate, thus, we can view an array with a non-broadside transmitter as a projected array with a broadside transmitter.

Another notable observation is that as the azimuth angle φ approaches $\pi/2$ (end-fire direction), the aperture length of the projected array, denoted as $D_{\text{array}}^{\text{proj}}$, approaches the height of the original array, which is ℓ . Mathematically, we can express it as $\lim_{\varphi \rightarrow \pi/2} (\sqrt{\ell^2 + (w \cdot \cos(\varphi))^2}) = \ell$. If $c \rightarrow \infty$ (corresponding to a horizontal ULA), then $\ell \rightarrow 0$. According to Theorem 2 in this scenario, the 3 dB BD will tend towards infinity because the denominator shrinks much faster

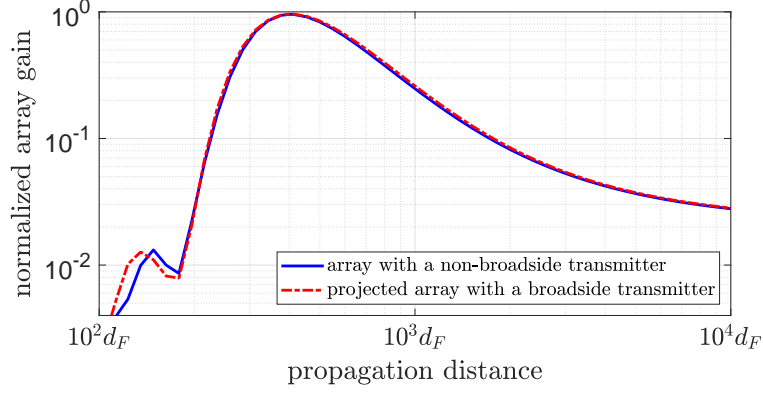
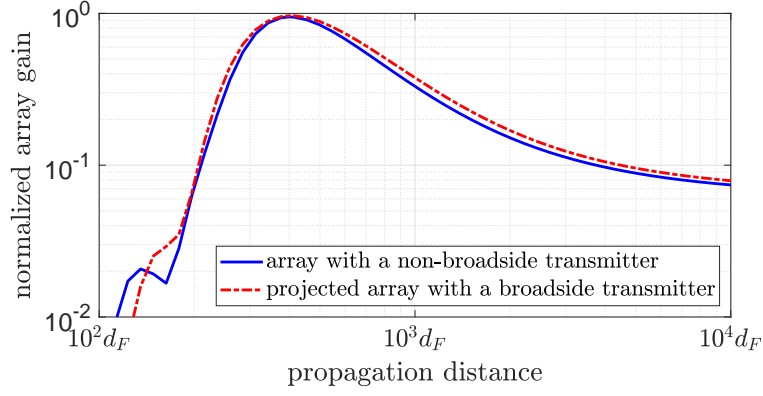
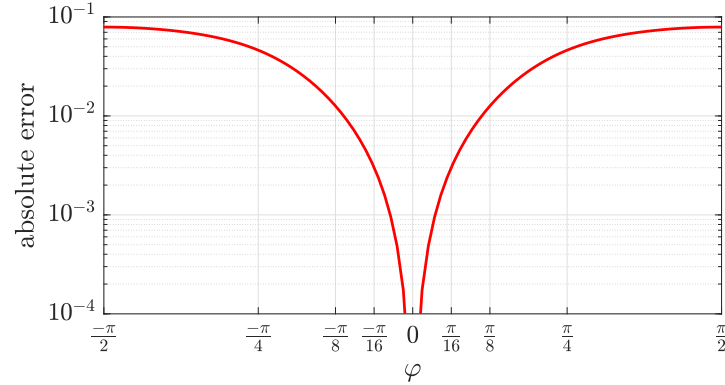
(a) The normalized array gain versus the propagation distance, $\varphi = \pi/8$.(b) The normalized array gain versus the propagation distance, $\varphi = \pi/4$.(c) The approximation error versus the azimuth angle, $d = 1000d_F$.

Fig. 13. The normalized array gain achieved by a square array with a non-broadside transmitter can be approximated by a projected rectangular array with a broadside transmitter. We set $F = d_B = 400d_F$, $f_c = 3$ GHz, and $N = 10^4$.

than the numerator, due to the dominant factor $d_{FA}^2 = \left(\frac{2(D_{\text{array}}^{\text{proj}})^2}{\lambda} \right)^2$. This observation is consistent with the findings illustrated in Fig. 10, which shows that the BD increases when $\varphi \rightarrow \pi/2$, and tends towards infinity when φ approaches $\pi/2$ and c is much larger than 1. We summarize the findings as follows.

Observation 4. We can approximate the gain of a rectangular array with a non-broadside transmitter using a smaller/projected array with a broadside transmitter. Moreover, as the transmitter approaches the end-fire direction of the array, the BD grows and approaches infinity as c becomes much greater than 1.

V. GAIN AND BEAM DEPTH OF A CIRCULAR ARRAY

In this section, we consider a UPA with a circular shape. The antenna elements are uniformly distributed across the array. Although there are numerous ways to distribute the antenna elements in a circular array evenly, we simplify things by assuming that each element is sufficiently small to ensure that the particular configuration of the elements has little impact on the array's overall gain. This presumption relies on the idea that the antenna elements in the array will radiate in a roughly symmetrical way. The Fresnel approximation of the normalized array gain for a circular array with a transmitter located at $(0, 0, z)$ and the focus point at $(0, 0, F)$, is computed using (8) with $E(x, y)$ in (11) and inject the phase-shift $e^{+j\frac{2\pi}{\lambda}\left(\frac{x^2}{2F} + \frac{y^2}{2F}\right)}$. Due to the circular geometry of the array, we adopt a polar coordinate system in the following analysis. In particular, the polar coordinate enables us to simplify the derivations of the Fresnel approximation.

A. Gain and 3 dB Beam Depth

We will now analyze the normalized array gain and BD of the circular array. Assuming that the phase shifts are perfectly compensated by continuous matched filtering. When we inject a phase shift to focus the array on a certain propagation distance, the normalized array gain can be approximated using the Fresnel approximation, given in the following theorem.

Theorem 4. When the transmitter is located at $(0, 0, z)$ and the matched filtering is focused on $(0, 0, F)$, the normalized array gain for the circular array can be approximated using the Fresnel approximation as

$$\hat{G}_{\text{circ}} = \text{sinc}^2(\tilde{c}), \quad (21)$$

where $\tilde{c} = \frac{R^2}{2\lambda z_{\text{eff}}}$ and $R = D/2 = \lambda/8$ is the radius of the circular array, which matches the aperture length of the rectangular array.

Proof. The proof is provided in Appendix C and is inspired by [27]. □

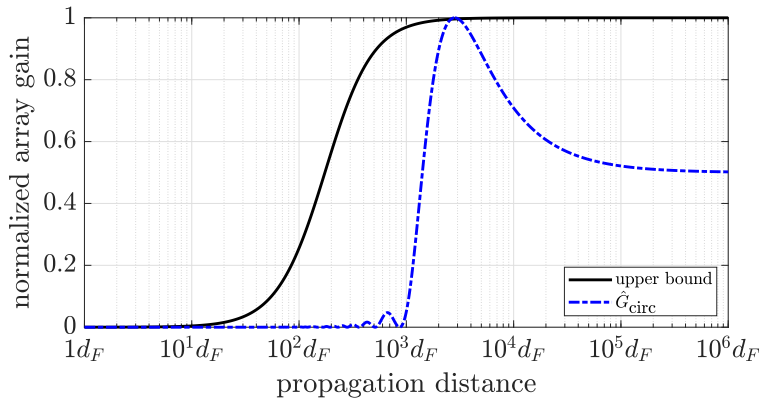


Fig. 14. The normalized circular array gain versus the propagation distance.

The 3 dB BD for the circular array when focusing on a point $F \geq d_B$ can then be calculated based on (21).

Theorem 5. The 3 dB BD of a circular array with a matched filter focused on $(0, 0, F)$, where $F \geq d_B$, is computed as

$$\text{BD}_{3\text{dB}}^{\text{circ}} = \begin{cases} \frac{1.7720R^2 F^2 \lambda}{R^4 - (0.886\lambda F)^2}, & F < \frac{R^2}{0.886\lambda}, \\ \infty, & F \geq \frac{R^2}{0.886\lambda}. \end{cases} \quad (22)$$

Proof. We know that $\text{sinc}^2(0) = 1$ and $\text{sinc}^2(0.4430) \approx 0.5$. The 3 dB BD $\text{BD}_{3\text{dB}}^{\text{circ}}$ is defined as the range of distances where the gain is greater than 0.5, therefore, it is the difference of two possible values of z , i.e., $\frac{R^2 F}{R^2 - 0.886\lambda F} - \frac{R^2 F}{R^2 + 0.886\lambda F}$ which results in (22). \square

The finite BD limit for the circular array is $\frac{R^2}{0.886\lambda}$, since the BD goes to infinity when the focus is on a point larger than the finite BD limit. We evaluate the normalized array gain of the circular array in Fig. 14. We can see that we approach -3 dB as $z \rightarrow \infty$, and hence the finite BD limit $\frac{R^2}{0.886\lambda}$ is the largest distance in which the BD for which the BD is finite.

If we adjust the focus to $F = d_B = 2(2R)$ and keep the array's aperture length the same as in the case of a rectangular array (i.e., $R = D/2$), then we obtain the BD for the circular array as $\text{BD}_{3\text{dB}}^{\text{circ}} \approx 247d_F$, according to Theorem 5. The BD is slightly higher as compared to the $\text{BD}_{3\text{dB}}^{\text{rect}} \approx 244d_F$ in Theorem 2 for tall $c = 0.1$ or wide $c = 10$ rectangular arrays.

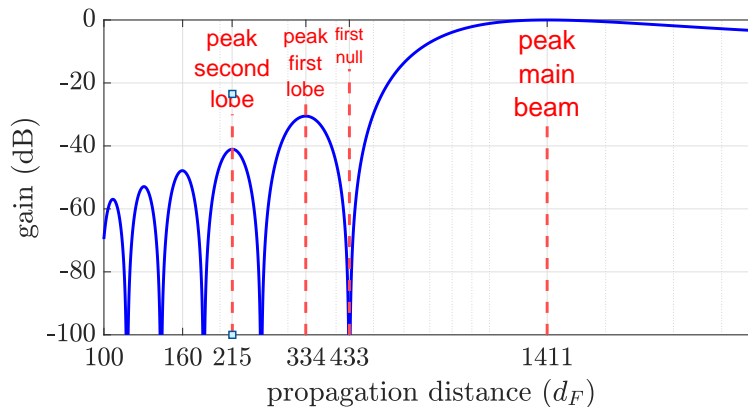
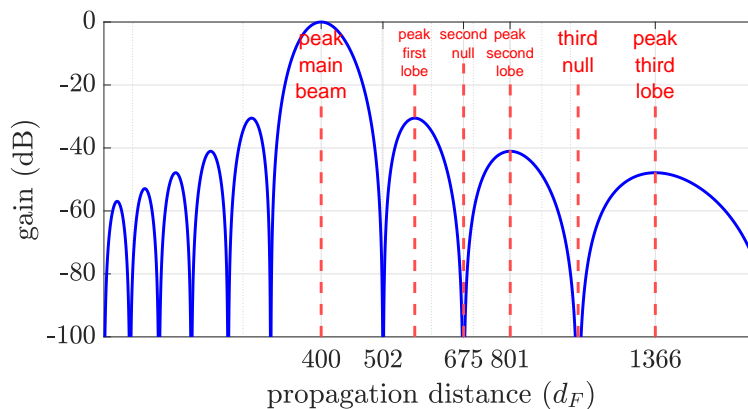
(a) The nulls and side-lobes for a circular array, $F = \frac{R^2}{0.886\lambda}$.(b) The nulls and side-lobes for a circular array, $F = d_B$.

Fig. 15. The array gains, nulls, and side-lobes with respect to the propagation distance with a circular array.

Sinc constant $\tilde{c} = \frac{R^2}{2\lambda z_{\text{eff}}}$	Gain (dB)	Explanation
0	0	peak of main beam
1	$-\infty$	first null
1.43	-30.54	peak of first lobe
2	$-\infty$	second null
2.46	-41.06	peak of second lobe
3	$-\infty$	third null
3.47	-47.87	peak of third lobe

TABLE I
SUMMARY OF NULLS AND SIDE-LOBES IN THE DEPTH DOMAIN WITH A CIRCULAR ARRAY.

B. Nulls and Side-lobes in the Depth Domain

When beams are analyzed in the angular domain, they are known to consist of a main beam and multiple weaker side-lobes, with nulls in between. The same behavior appears in the depth domain when considering finite-depth beamforming. We will now investigate the nulls and side-

lobes for the circular array based on the approximate gain in (21). The peak of the main beam in the depth domain appears when $\tilde{c} = 0$ so that $\left(\frac{\sin(\tilde{c})}{\tilde{c}}\right)^2 = 1$. Since $\tilde{c} = \frac{\pi R^2}{2\lambda z_{\text{eff}}}$, it equals to 0 when $z_{\text{eff}} = \infty$ which implies that $F = z$. Therefore, the peak of the main beam is obtained at the distance $F = z$. The first null appears when $\tilde{c} = \pi$. Hence, $z_{\text{eff}} = \frac{R^2}{2\lambda}$. The second and later nulls appear when $\tilde{c} = 2\pi, \dots, K\pi$. Therefore, the nulls can be obtained by setting $z_{\text{eff}} = \frac{k_0 R^2}{2\lambda}$, where $k_0 \in \{1, \dots, K\}$ indicates the index of the nulls. The peak values of the side-lobes is given in Table I. We plot Fig. 15 to demonstrate the nulls and side-lobes of the circular array. The characterization of the nulls and beamdepths in Table I match the nulls and beamdepths in Fig. 15.

VI. CONCLUSION

In this paper, we analyzed how the BD of a large planar rectangular array depends on its width-to-height proportion, area, and aperture length. We derived a tight Fresnel approximation of the normalized array gain and used it to characterize the BD of the rectangular array. We proved that the 3 dB BD is the largest for a square array. The BD pattern is symmetric for tall and wide arrays. The smallest BD is obtained when the array approaches a ULA. Therefore, an array of linear geometry is preferred since it offers the smallest BD, enabling us to better utilize spatial multiplexing since there is a higher degree of spatial orthogonality (in the distance domain). The array's aperture length has a more significant impact on the BD and finite BD limit than the aperture area. We also considered a projected square array where its effective aperture length is shorter than the original square array due to the rotation. We then considered a non-broadside transmitter, where we first evaluated the Taylor approximation of the Euclidean between the transmitter and the antenna element of the array. We refined the approximation so that the approximation error decreases with the increase of the propagation distance. When the width-to-height proportion approaches zero, the BD becomes independent of the azimuth angles. For larger width-to-height proportions, the BD increases with increasing azimuth angle. In addition, as the value of width-to-height proportion c increases, the BD variation also increases. Furthermore, we demonstrated that the beam pattern of an array with a non-broadside transmitter can be approximated by that of a projected/smaller array with a broadside transmitter. The original array was projected onto a plane that is perpendicular to the axis of the non-broadside transmitter. Finally, we considered a UPA with a circular shape. We derived the analytical Fresnel approximation of the normalized array gain and characterized the 3 dB BD. The BD of the

circular array is slightly larger compared to that of the wide/tall rectangular array, but lower than the square array. Our analysis also involved characterizing the nulls and side lobes of the circular array that emerge at different propagation distances.

APPENDIX A

PROOF OF THEOREM 1

First, we substitute the Fresnel approximation in (11) into the normalized array gain in (8) and inject phase-shift $e^{+j\frac{2\pi}{\lambda}\left(\frac{x^2}{2F} + \frac{y^2}{2F}\right)}$, which gives us

$$\begin{aligned} \hat{G}_{\text{rect}}(c) &= \frac{1}{(NA)^2} \left| \int_{-\frac{D_{\text{array}}}{2\sqrt{1+c^2}}}^{\frac{D_{\text{array}}}{2\sqrt{1+c^2}}} \int_{-\frac{cD_{\text{array}}}{2\sqrt{1+c^2}}}^{\frac{cD_{\text{array}}}{2\sqrt{1+c^2}}} e^{+j\frac{2\pi}{\lambda}\left(\frac{x^2}{2F} + \frac{y^2}{2F}\right)} e^{-j\frac{2\pi}{\lambda}\left(z + \frac{x^2}{2z} + \frac{y^2}{2z}\right)} dx dy \right|^2 \\ &= \frac{1}{(NA)^2} \left| \int_{-\frac{D_{\text{array}}}{2\sqrt{1+c^2}}}^{\frac{D_{\text{array}}}{2\sqrt{1+c^2}}} \int_{-\frac{cD_{\text{array}}}{2\sqrt{1+c^2}}}^{\frac{cD_{\text{array}}}{2\sqrt{1+c^2}}} e^{-j\frac{2\pi}{\lambda}\frac{(F-z)(x^2+y^2)}{2zF}} dx dy \right|^2. \end{aligned} \quad (23)$$

By defining $z_{\text{eff}} = \frac{Fz}{F-z}$, we can rewrite the expression as

$$\hat{G}_{\text{rect}}(c) = \frac{1}{(NA)^2} \left| \int_{-\frac{D_{\text{array}}}{2\sqrt{1+c^2}}}^{\frac{D_{\text{array}}}{2\sqrt{1+c^2}}} \int_{-\frac{cD_{\text{array}}}{2\sqrt{1+c^2}}}^{\frac{cD_{\text{array}}}{2\sqrt{1+c^2}}} e^{-j\frac{\pi}{\lambda}\frac{x^2}{z_{\text{eff}}}} e^{-j\frac{\pi}{\lambda}\frac{y^2}{z_{\text{eff}}}} dx dy \right|^2. \quad (24)$$

The evaluation of the anti-derivatives in (24) yields [26]

$$\begin{aligned} \hat{G}_{\text{rect}}(c) &= \left(\frac{4z_{\text{eff}}(1+c^2)}{cd_{FA}} \right)^2 \left(C^2 \left(c\sqrt{\frac{d_{FA}}{4z_{\text{eff}}(1+c^2)}} \right) + S^2 \left(c\sqrt{\frac{d_{FA}}{4z_{\text{eff}}(1+c^2)}} \right) \right) \\ &\quad C^2 \left(\sqrt{\frac{d_{FA}}{4z_{\text{eff}}(1+c^2)}} \right) + S^2 \left(\sqrt{\frac{d_{FA}}{4z_{\text{eff}}(1+c^2)}} \right), \end{aligned} \quad (25)$$

where $C(\cdot)$ and $S(\cdot)$ are the Fresnel integrals. By defining $a = \frac{d_{FA}}{4z_{\text{eff}}(1+c^2)}$, we finally obtain

$$\hat{G}_{\text{rect}}(c) = \frac{(C^2(c\sqrt{a}) + S^2(c\sqrt{a}))(C^2(\sqrt{a}) + S^2(\sqrt{a}))}{(ca)^2}. \quad (26)$$

This completes the proof.

APPENDIX B
PROOF OF THEOREM 3

For a transmitter located at $(x_t, 0, z)$, we use the Fresnel approximation based on (16), as

$$E(x, y) \approx \frac{E_0}{\sqrt{4\pi z}} e^{-j\frac{2\pi}{\lambda} \left(d + \frac{x^2 + y^2 - 2xx_t}{2d} \right)}. \quad (27)$$

Substituting (27) into the normalized array gain in (8) and inject phase-shift $e^{+j\frac{2\pi}{\lambda} \left(\frac{x^2}{2F} + \frac{y^2}{2F} \right)}$ yields

$$\begin{aligned} \tilde{G}_{\text{rect}}(c, \varphi) &= \frac{1}{(NA)^2} \left| \int_{-\frac{D_{\text{array}}}{2\sqrt{1+c^2}} - \frac{D_{\text{array}}}{2\sqrt{1+c^2}}}^{\frac{D_{\text{array}}}{2\sqrt{1+c^2}} - \frac{cD_{\text{array}}}{2\sqrt{1+c^2}}} \int_{-\frac{D_{\text{array}}}{2\sqrt{1+c^2}} - \frac{cD_{\text{array}}}{2\sqrt{1+c^2}}}^{\frac{D_{\text{array}}}{2\sqrt{1+c^2}} - \frac{cD_{\text{array}}}{2\sqrt{1+c^2}}} e^{j\frac{2\pi}{\lambda} \left(\frac{x^2}{2F} + \frac{y^2}{2F} \right)} e^{-j\frac{2\pi}{\lambda} \left(d + \frac{x^2 + y^2 - 2xx_t}{2d} \right)} dx dy \right|^2 \\ &= \frac{1}{(NA)^2} \left| \int_{-\frac{D_{\text{array}}}{2\sqrt{1+c^2}} - \frac{cD_{\text{array}}}{2\sqrt{1+c^2}}}^{\frac{D_{\text{array}}}{2\sqrt{1+c^2}} - \frac{cD_{\text{array}}}{2\sqrt{1+c^2}}} \int_{-\frac{D_{\text{array}}}{2\sqrt{1+c^2}} - \frac{cD_{\text{array}}}{2\sqrt{1+c^2}}}^{\frac{D_{\text{array}}}{2\sqrt{1+c^2}} - \frac{cD_{\text{array}}}{2\sqrt{1+c^2}}} e^{-j\frac{\pi}{\lambda} \left(\frac{x^2}{d_{\text{eff}}} + 2\frac{xx_t}{d} \right)} e^{-j\frac{\pi}{\lambda} \left(\frac{y^2}{d_{\text{eff}}} \right)} dx dy \right|^2 \\ &= \left(\frac{\lambda d_{\text{eff}} (1+c^2)}{\pi c N D^2} \right)^2 \left| \int_{-\sqrt{\frac{\pi}{\lambda d_{\text{eff}}}} \frac{D_{\text{array}}}{2\sqrt{1+c^2}} - \sqrt{\frac{\pi}{\lambda d_{\text{eff}}}} \frac{cD_{\text{array}}}{2\sqrt{1+c^2}} + \frac{x_t}{d} \sqrt{\frac{\lambda d_{\text{eff}}}{\pi}}}^{\sqrt{\frac{\pi}{\lambda d_{\text{eff}}}} \frac{D_{\text{array}}}{2\sqrt{1+c^2}} - \sqrt{\frac{\pi}{\lambda d_{\text{eff}}}} \frac{cD_{\text{array}}}{2\sqrt{1+c^2}} + \frac{x_t}{d} \sqrt{\frac{\lambda d_{\text{eff}}}{\pi}}} \int_{-\sqrt{\frac{\pi}{\lambda d_{\text{eff}}}} \frac{D_{\text{array}}}{2\sqrt{1+c^2}} - \sqrt{\frac{\pi}{\lambda d_{\text{eff}}}} \frac{cD_{\text{array}}}{2\sqrt{1+c^2}} + \frac{x_t}{d} \sqrt{\frac{\lambda d_{\text{eff}}}{\pi}}}^{\sqrt{\frac{\pi}{\lambda d_{\text{eff}}}} \frac{D_{\text{array}}}{2\sqrt{1+c^2}} - \sqrt{\frac{\pi}{\lambda d_{\text{eff}}}} \frac{cD_{\text{array}}}{2\sqrt{1+c^2}} + \frac{x_t}{d} \sqrt{\frac{\lambda d_{\text{eff}}}{\pi}}} e^{-ju^2} e^{-jv^2} dudv \right|^2, \quad (28) \end{aligned}$$

where $u = \sqrt{\frac{\pi}{\lambda d_{\text{eff}}}} x + \frac{x_t}{d} \sqrt{\frac{\lambda d_{\text{eff}}}{\pi}}$, $v = \sqrt{\frac{\pi}{\lambda d_{\text{eff}}}} y$, and $d_{\text{eff}} = \frac{Fd}{|F-d|}$. By using the Euler formula, i.e., $e^{jx} = \cos(x) + j\sin(x)$, we can compute (28) and get

$$\begin{aligned} \tilde{G}_{\text{rect}}(c, \varphi) &= \left(\frac{1}{2cp^2} \right)^2 \left| \left((C(cp+q) - C(-cp+q)) - j(S(cp+q) - S(-cp+q)) \right) \right. \\ &\quad \left. \left((C(p) - C(-p)) - j(S(p) - S(-p)) \right) \right|^2, \quad (29) \end{aligned}$$

where $p = D\sqrt{\frac{N}{2\lambda d_{\text{eff}}(1+c^2)}}$ and $q = \frac{x_t}{d\pi} \sqrt{2\lambda d_{\text{eff}}} = \frac{\sin(\varphi)}{\pi} \sqrt{2\lambda d_{\text{eff}}}$. Since $D = \sqrt{\frac{\lambda d_F}{2}}$ and $C(-v) = -C(v)$ due to the odd function [26], we can rewrite (29) as

$$\begin{aligned} \tilde{G}_{\text{rect}}(c, \varphi) &= \left(\frac{1}{2cp^2} \right)^2 \left| \left(C(cp+q) + C(cp-q) - j(S(cp+q) + S(cp-q)) \right) \left(C(p) - jS(p) \right) \right|^2 \\ &= \frac{(C^2(p) + S^2(p))}{(2cp^2)^2} \left((C(cp+q) + C(cp-q))^2 + (S(cp+q) + S(cp-q))^2 \right), \quad (30) \end{aligned}$$

where $p = \frac{1}{2} \sqrt{\frac{d_{FA}}{d_{\text{eff}}(1+c^2)}}$, which completes the proof.

APPENDIX C

PROOF OF THEOREM 4

We first substitute the Fresnel approximation in (11) into the normalized array gain in (8) and inject phase-shift $e^{+j\frac{2\pi}{\lambda}\left(\frac{x^2}{2F} + \frac{y^2}{2F}\right)}$. Then, we use a polar coordinate system to represent the multiple integrations in (8), explained in [28, Section 6]. We can write the Fresnel approximation of the normalized array gain for the circular array as

$$\tilde{G}_{\text{circ}} = \frac{1}{(\pi R^2)^2} \left| \int_0^{2\pi} \int_0^R r e^{j\frac{2\pi}{\lambda}\left(F + \frac{r^2}{2F}\right)} e^{-j\frac{2\pi}{\lambda}\left(z + \frac{r^2}{2z}\right)} dr d\varphi \right|^2 = \frac{1}{(\pi R^2)^2} \left| 2\pi \int_0^R r e^{-j\frac{\pi}{\lambda} \frac{r^2}{z_{\text{eff}}}} dr \right|^2, \quad (31)$$

where $z_{\text{eff}} = \frac{Fz}{|F-z|}$. Substituting $u = -j\frac{\pi r^2}{\lambda z_{\text{eff}}}$, we can rewrite \tilde{G}_{circ} as

$$\begin{aligned} \tilde{G}_{\text{circ}} &= \left(\frac{1}{\pi R^2} \right)^2 \left| j\lambda z_{\text{eff}} \int_0^{-j\frac{\pi R^2}{\lambda z_{\text{eff}}}} e^u du \right|^2 = \left(\frac{1}{\pi R^2} \right)^2 \left| \lambda z_{\text{eff}} \left(\sin \left(\frac{\pi R^2}{\lambda z_{\text{eff}}} \right) + \left(\cos \left(\frac{\pi R^2}{\lambda z_{\text{eff}}} \right) - 1 \right) j \right) \right|^2 \\ &= \left(\frac{\lambda z_{\text{eff}}}{\pi R^2} \right)^2 \left(2 - 2 \cos \left(\frac{\pi R^2}{\lambda z_{\text{eff}}} \right) \right) = \left(\frac{\sin(\tilde{c})}{\tilde{c}} \right)^2, \end{aligned}$$

where $\tilde{c} = \frac{\pi R^2}{2\lambda z_{\text{eff}}}$. This completes the proof.

REFERENCES

- [1] A. Kosasih and E. Björnson, "Beam depth analysis for large rectangular arrays," in *Proc. IEEE Global Commun. Conf.*, 2023, submitted for publication.
- [2] T. S. Rappaport, S. Sun, R. Mayzus, H. Zhao, Y. Azar, K. Wang, G. N. Wong, J. K. Schulz, M. Samimi, and F. Gutierrez, "Millimeter wave mobile communications for 5G cellular: It will work!" *IEEE Access*, vol. 1, p. 335–349, May 2013.
- [3] A. Amiri, M. Angelichinoski, E. de Carvalho, and R. W. Heath, "Extremely large aperture massive MIMO: Low complexity receiver architectures," in *Proc. IEEE Global Commun. Conf. Workshops*, UAE, Dec. 2018.
- [4] H. Wang, A. Kosasih, C. -K. Wen, S. Jin and W. Hardjawana, "Expectation propagation detector for extra-large scale massive MIMO," *IEEE Trans. Wireless Commun.*, vol. 19, no. 3, pp. 2036–2051, Mar. 2020.
- [5] A. Pizzo, T. L. Marzetta, and L. Sanguinetti. (2019) Spatially-stationary model for holographic MIMO small-scale fading. [Online]. Available: <https://arxiv.org/abs/1911.04853>, preprint.
- [6] T. S. Rappaport et al., "Wireless communications and applications above 100 GHz: Opportunities and challenges for 6G and beyond," *IEEE Access*, vol. 7, pp. 78 729–78 757, June 2019.
- [7] L. Sanguinetti, E. Björnson, and J. Hoydis, "Toward massive MIMO 2.0: Understanding spatial correlation, interference suppression, and pilot contamination," *IEEE J. Sel. Areas Commun.*, vol. 68, no. 1, p. 232–257, Jan 2020.

- [8] E. Björnson, L. Sanguinetti, H. Wymeersch, J. Hoydis, and T. L. Marzetta, “Massive MIMO is a reality—What is next? Five promising research directions for antenna arrays,” *Dig. Sig. Process.*, vol. 94, p. 3–20, Nov. 2019.
- [9] J. Zhang, E. Björnson, M. Matthaiou, D. W. K. Ng, H. Yang, and D. J. Love, “Prospective multiple antenna technologies for beyond 5G,” *IEEE J. Sel. Areas Commun.*, vol. 38, no. 8, p. 1637–1660, Aug. 2020.
- [10] W. Tang et al., “Wireless communications with reconfigurable intelligent surface: Path loss modeling and experimental measurement,” *IEEE Trans. Wireless Commun.*, vol. 20, no. 1, pp. 421–439, Jan. 2021.
- [11] P. Ramezani and E. Björnson. (2022) Near-field beamforming and multiplexing using extremely large aperture arrays. [Online]. Available: <https://arxiv.org/abs/2209.03082>, preprint.
- [12] J. Sherman, “Properties of focused apertures in the Fresnel region,” *IRE Trans. Antennas Propag.*, vol. 10, no. 4, p. 399–408, July 1962.
- [13] H. Lu and Y. Zeng, “Communicating with extremely large-scale array/surface: Unified modeling and performance analysis,” *IEEE Trans. Wireless Commun.*, vol. 21, no. 6, pp. 4039–4053, June 2022.
- [14] A. d. J. Torres, L. Sanguinetti and E. Björnson, “Near- and far-field communications with large intelligent surfaces,” in *Proc. 54th Asilomar Conf. on Signal, Syst., and Comput.*, USA, Nov 2020, pp. 564–568.
- [15] J. Yang , Y. Zeng , S. Jin , C.-K. Wen , and P. Xu, “Communication and localization with extremely large lens antenna array,” *IEEE Trans. Wireless Commun.*, vol. 20, no. 5, pp. 3031–3048, Jan 2021.
- [16] Y. Jiang, F. Gao, M. Jian, S. Zhang, and W. Zhang, “Reconfigurable intelligent surface for near field communications: Beamforming and sensing,” *IEEE Trans. Wireless Commun.*, vol. Early Access, Nov. 2022.
- [17] M. Cui and L. Dai. (2022) Channel Estimation for extremely large-scale MIMO: Far-field or near-field? [Online]. Available: <https://arxiv.org/abs/2108.07581>, preprint.
- [18] Z. Wu and L. Dai. (2023) Multiple access for near-field communications: SDMA or LDMA? [Online]. Available: <https://arxiv.org/abs/2208.06349>, preprint.
- [19] N. J. Myers and R. W. Heath, “InFocus: A spatial coding technique to mitigate misfocus in near-field LoS beamforming,” *IEEE Trans. Wireless Commun.*, vol. 21, no. 4, pp. 2193–2209, Apr. 2022.
- [20] N. Deshpande, M. R. Castellanos, S. R. Khosravirad, J. Du, H. Viswanathan, and R. W. Heath, “A wideband generalization of the near-field region for extremely large phased-arrays,” *IEEE Wireless Commun. Lett.*, vol. 12, no. 3, pp. 515–519, March 2023.
- [21] E. Björnson, Ö. T. Demir, and L. Sanguinetti, “A Primer on near-field beamforming for arrays and reconfigurable intelligent surfaces,” in *Proc. IEEE 55th Asilomar Conf. on Signal, Syst., and Comput.*, USA, Nov. 2021, pp. 105–112.
- [22] S. Hu, F. Rusek, and O. Edfors, “Beyond massive MIMO: The potential of data transmission with large intelligent surfaces,” *IEEE Trans. on Signal Proc.*, vol. 66, no. 10, pp. 2746–2758, 2018.
- [23] D. Dardari, “Communicating with large intelligent surfaces: Fundamental limits and models,” *IEEE J. Sel. Areas in Commun.*, vol. 38, no. 11, pp. 2526–2537, 2020.
- [24] E. Björnson and L. Sanguinetti, “Power scaling laws and near-field behaviors of massive MIMO and intelligent reflecting surfaces,” *IEEE Open J. of the Commun. Soc.*, vol. 1, pp. 1306–1324, Sept. 2020.
- [25] A. Kay, “Near-field gain of aperture antennas,” *IRE Trans. Antennas Propag.*, vol. 8, no. 6, pp. 586–593, Nov. 1960.
- [26] C. Polk, “Optical Fresnel-Zone gain of a rectangular aperture,” *IRE Trans. Antennas Propag.*, vol. 4, no. 1, pp. 65–69, Jan. 1956.
- [27] S. Silver, *Microwave antenna theory and design*. The Institution of Engineering and Technology (IET), 1984.
- [28] S. J. B. K. F. Riley, M. P. Hobson, *Mathematical methods for physics and engineering: A comprehensive guide*. Cambridge University Press, 2006.